VIP Photovoltaic Devices Very Important Paper

Deutsche Ausgabe: DOI: 10.1002/ange.201600702
Internationale Ausgabe: DOI: 10.1002/anie.201600702

Monodisperse Dual-Functional Upconversion Nanoparticles Enabled Near-Infrared Organolead Halide Perovskite Solar Cells

*Ming He, Xinchang Pang, Xueqin Liu, Beibei Jiang, Yanjie He, Henry Snaith, and Zhiqun Lin**

Abstract: *Extending the spectral absorption of organolead halide perovskite solar cells from visible into near-infrared (NIR) range renders the minimization of non-absorption loss of solar photons with improved energy alignment. Herein, we report on, for the first time, a viable strategy of capitalizing on judiciously synthesized monodisperse $NaYF_4$:Yb/Er upconversion nanoparticles (UCNPs) as the mesoporous electrode for $CH_3NH_3PbI_3$ perovskite solar cells and more importantly confer perovskite solar cells to be operative under NIR light. Uniform $NaYF_4$:Yb/Er UCNPs are first crafted by employing rationally designed double hydrophilic star-like poly(acrylic acid)-block-poly(ethylene oxide) (PAA-b-PEO) diblock copolymer as nanoreactor, imparting the solubility of UCNPs and the tunability of film porosity during the manufacturing process. The subsequent incorporation of $NaYF_4$:Yb/Er UCNPs as the mesoporous electrode led to a high efficiency of 17.8%, which was further increased to 18.1% upon NIR irradiation. The in situ integration of upconversion materials as functional components of perovskite solar cells offers the expanded flexibility for engineering the device architecture and broadening the solar spectral use.*

Recent research has witnessed unprecedented advances in organolead halide perovskite solar cells with a power conversion efficiency (PCE) leaping from approximately 3% to over 20%.[1–5] Several strategies have been successfully developed for improving PCE of organolead halide perovskite solar cells, for example, by controlling the crystallization of perovskite active layers,[6] engineering the interface energy alignments,[7,8] and modifying the chemical composition of perovskites.[9,10] The standard spectrum of AM1.5G sunlight ranges from 280 nm to 2500 nm (i.e., 0.5–4.4 eV), however, only a small fraction of incident photons in the UV and visible ranges (280 nm to 800 nm) can be absorbed and converted into electricity in perovskite solar cells.[11] A large portion of the incident light is thus lost in the form of thermalization and non-absorption photons. One promising approach to decrease such non-absorption photon loss is the employment of UCNPs to preferably harvest the NIR solar photons, followed by the absorption of emitted high-energy photons to generate extra photocurrent in solar cells, offering a potential means of overcoming the Shockley–Queisser limit of a single-junction solar cell.[12]

Theoretical calculations have predicted that the PCE of a typical silicon solar cell ($E_g = 1.1$ eV) can be increased from 20% to 25% by putting a rear UCNP layer under concentrated solar power.[13,14] For practical interest, ytterbium/erbium-doped lanthanum fluoride (LaF_3:Yb/Er) UCNPs have been integrated with TiO_2 as the internal mesoporous electrode in dye-sensitized solar cells (DSSCs) to enable the absorption of NIR light. However, this internal configuration of LaF_3:Yb/Er-TiO_2 nanocomposites suffered from large charge recombination at the LaF_3:Yb/Er-TiO_2/dye/electrolyte interfaces.[15] In sharp contrast to liquid electrolyte-based DSSCs, organolead halide perovskite solar cells exhibit a strong compatibility with a variety of electrode materials owing to their highly efficient ambipolar charge transport nature. In this context, insulating UCNPs may be exploited as internal mesoporous electrode and in the meantime entail organolead halide perovskite solar cells to work under NIR light. However, this has yet to be explored.

One prerequisite for practical applications of UCNPs invokes the surface modification with organic ligands, which ultimately determine the dispersibility and stability of these nanoparticles in solvents. Clearly, an intimate interfacial contact between UCNPs and ligands is crucial for achieving long-term stable dispersion of UCNPs in solvents. A large number of impressive approaches, such as ligand exchange,[16] direct grafting,[17–20] and direct nanocrystal growth,[21] have demonstrated the feasibility of realizing the intimate contact between them. However, organic ligands may dissociate from the surface of inorganic nanoparticles over a long period of time, as they are often not connected permanently with each other and there is a weak interaction or not strong enough binding between them. The surface ligands also influence the nanoparticle spacing. The aiblity to tune the porosity of mesoporous structures is key to high-performance materials and devices, for example, lithium batteries, drug delivery, pollutant filtration, and gas storage.

Herein, we report for the first time an unconventional route to monodisperse $NaYF_4$:Yb/Er UCNPs as the mesoporous electrode for NIR organolead halide perovskite solar cells. Uniform $NaYF_4$:Yb/Er UCNPs permanently tethered with hydrophilic polymer as surface ligands were first crafted by capitalizing on a rationally designed double hydrophilic star-like poly(acrylic acid)-*block*-poly(ethylene oxide) (PAA-*b*-PEO) diblock copolymer as a nanoreactor through the strong coordination interaction between the carboxyl func-

[*] Dr. M. He, Dr. X. Pang, X. Liu, B. Jiang, Y. He, Prof. Z. Lin
School of Materials Science and Engineering, Georgia Institute of Technology
Atlanta, GA 30332 (USA)
E-mail: zhiqun.lin@mse.gatech.edu
Homepage: http://nanofm.mse.gatech.edu/
Prof. H. Snaith
Clarendon Laboratory, Department of Physics
University of Oxford
Parks Road, Oxford, OX1 3PU (UK)

Supporting information for this article can be found under http://dx.doi.org/10.1002/anie.201600702.

tional groups of inner PAA blocks and the metal moieties of precursors of $NaYF_4$:Yb/Er. The outer PEO blocks render the solubility and long-term stability of the resulting $NaYF_4$:Yb/Er UCNPs in aqueous solution, and offer the capability of adjusting the porosity by introducing PEO homopolymer as additives. The $NaYF_4$:Yb/Er mesoporous electrode was demonstrated to enable the NIR $CH_3NH_3PbI_3$ perovskite solar cell by converting the low-energy NIR photons into absorbable high-energy visible photons.

The synthetic route to hydrophilic PEO-capped $NaYF_4$:Yb/Er UCNPs using the double hydrophilic star-like PAA-*b*-PEO diblock copolymer as a nanoreactor is depicted in Figure 1. The star-like PAA-*b*-PEO diblock copolymer was synthesized by atom transfer radical polymerization (ATRP) of *tert*-butyl acrylate using 21Br-β-CD as a macroinitiator, followed by a click reaction with alkyne-terminated PEO and hydrolysis in trifluoroacetic acid (see the Methods Section in the Supporting Information, Figures S1–S3).[22,23] The strong coordination bonding between the carboxyl functional groups of PAA blocks and the rare-earth metallic ions of the $NaYF_4$:Yb/Er precursors (i.e., CF_3COONa, $Y(CF_3COO)_3$, $Yb(CF_3COO)_3$, and $Er(CF_3COO)_3$) allowed the preferential incorporation of precursors within the regime occupied by inner PAA blocks of the star-like PAA-*b*-PEO diblock copolymer. The thermal decomposition of rare-earth metallic trifluoroacetates within the nanoreactor at a relatively high temperature promoted the nucleation of $NaYF_4$:Yb/Er upconversion nanocrystals and finally grew into uniform $NaYF_4$:Yb/Er UCNPs. As the surface of the UCNPs are intimately covered by PEO blocks that are originally covalently bonded to inner PAA blocks, the $NaYF_4$:Yb/Er UCNPs possess an excellent solubility in hydrophilic solvents with long-term stability. More importantly, such direct capping of PEO chains on the surface of $NaYF_4$:Yb/Er UCNPs not only simplifies the purification process of the resulting nanoparticles because they dispense with the need for ligand exchange, but also facilitates the manufacturing of the $NaYF_4$:Yb/Er mesoporous electrode as the PEO ligands render the formation of relatively thick interlayers between UCNPs as compared with small molecular ligands, offering a potential route to relatively large-sized mesoporosity after the removal of the PEO ligands.

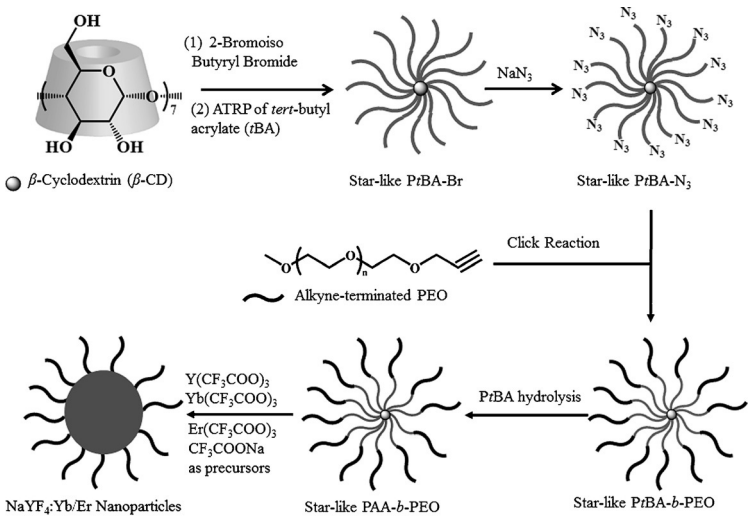

Figure 1. Scheme of the synthetic route to $NaYF_4$:Yb/Er upconversion nanoparticles (UCNPs) by capitalizing on the double hydrophilic star-like poly(acrylic acid)-*block*-poly(ethylene oxide) (PAA-*b*-PEO) diblock copolymer as a nanoreactor.

Figure 2a shows a representative transmission electron microscopy (TEM) image of high-quality, monodisperse $NaYF_4$:Yb/Er UCNPs with an average size of 16.3 ± 0.8 nm (i.e., the size distribution is less than 5% of its average size). The high-resolution TEM image in the inset revealed an interplanar lattice spacing of 0.52 nm, corresponding to the (100) crystal plane of hexagonal-phase $NaYF_4$:Yb/Er crystals. X-ray diffraction (XRD) measurement further substantiated the formation of hexagonal $NaYF_4$:Yb/Er crystals (Figure 2b). The PEO diffraction peaks appeared at 2θ of 19.2° and 23.3°,[24] while all other diffraction peaks can be readily indexed to hexagonal $NaYF_4$:Yb/Er crystals (JCPDS 00-028-1192). The average size of $NaYF_4$:Yb/Er UCNPs estimated from the XRD profile by the Scherrer equation was approximately 18.5 nm, which is comparable with the TEM result, indicating that the star-like PAA-*b*-PEO diblock copolymer template enabled the synthesis of highly crystalline uniform $NaYF_4$:Yb/Er UCNPs. Hexagonal-phase (β-phase) $NaYF_4$:Yb/Er is more favorable for upconversion applications because of its high upconversion quantum yield in comparison with its cubic-phase (α-phase) counterpart.[12] Figure 2c displays the upconversion fluorescence spectrum of $NaYF_4$:Yb/Er UCNPs under excitation by a 980 nm NIR laser. As illustrated in the inset, the upconversion transition of $NaYF_4$:Yb/Er is basically a nonlinear *anti*-Stokes optical process,[11,12] involving the excitation of Yb ions under NIR light, the energy transfer from Yb to Er ions, and the radiative energy decay of Er ions. Consequently, four emission peaks at 408, 523, 542, and 655 nm were observed, which are associated with the $^2H_{9/2}$–$^4I_{15/2}$, $^2H_{11/2}$–$^4I_{15/2}$, $^4S_{3/2}$–$^4I_{15/2}$, and $^4F_{9/2}$–$^4I_{15/2}$ transitions of Er ions, respectively.[25] Interestingly, strong green fluorescence, corresponding to $^2H_{11/2}$–$^4I_{15/2}$ and $^4S_{3/2}$–$^4I_{15/2}$ energy transitions was seen to be dominated for $NaYF_4$:Yb/Er UCNPs in both solution and solid state under 980 nm laser excitation (inset in Figure 2c).

The PEO-capped $NaYF_4$:Yb/Er UCNPs were then fabricated into mesoporous electrodes for $CH_3NH_3PbI_3$ perovskite solar cells, as schematically illustrated in Figure S4 (see the Methods Section in the Supporting Information). The $CH_3NH_3PbI_3$ perovskite layer was then deposited by a modified two-step method, forming $CH_3NH_3PbI_3$ cuboids with an average size of 340 nm,[26] and the cross-sectional SEM image showed that the $NaYF_4$:Yb/Er mesoporous layer was fully covered with $CH_3NH_3PbI_3$ (Figure S5). The inter-nanoparticle spacing (i.e., pore size) of the $NaYF_4$:Yb/Er mesoporous film can readily be tuned by adding a small amount of PEO homopolymer in the nanoparticle solution, leading to the increased inter-nanoparticle spacing in the mesoporous film

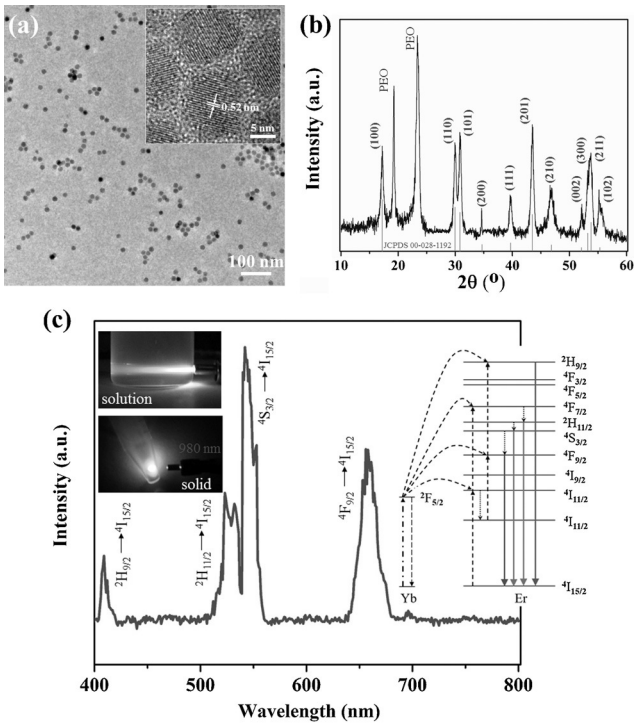

Figure 2. a) A representative transmission electron microscopy (TEM) image of $NaYF_4$:Yb/Er upconversion nanoparticles (UCNPs). Inset: High-resolution TEM image showing the $NaYF_4$:Yb/Er crystal lattices. b) X-ray diffraction (XRD) profile of $NaYF_4$:Yb/Er UCNPs. c) The upconversion fluorescence spectrum of $NaYF_4$:Yb/Er UCNPs under a 980 nm NIR laser excitation. The corresponding energy transitions are shown as an inset on the right. The left insets are the digital images of green fluorescence (convert into gray scale) emitted from $NaYF_4$:Yb/Er UCNPs under a 980 nm NIR laser irradiation in solution (top) and solid (bottom) states.

after oxygen plasma treatment. The pore size distribution and specific surface area of the $NaYF_4$:Yb/Er mesoporous films were characterized by a nitrogen gas sorption technique (Figure 3a,b). For the mesoporous film prepared from $NaYF_4$:Yb/Er UCNPs without the PEO additives, the average pore size was 23.6 nm and the surface area was 64.3 $cm^2 g^{-1}$ compared to a pore size of 27.9 nm and a surface area of 60.9 $cm^2 g^{-1}$, respectively, in the TiO_2 reference film (Figure S6). With the addition of 0.8 wt% extra PEO homopolymer, the average pore sizes of $NaYF_4$:Yb/Er mesoporous films can eventually be increased to 30.5 nm (Table S1). This is not surprising as the additional PEO homopolymer would preferentially segregate to the original PEO ligand phases that are tethered on the surface of $NaYF_4$:Yb/Er UCNPs, and expand the interparticle spacing of $NaYF_4$:Yb/Er UCNPs. The mesoporous structure collapsed after adding more PEO homopolymer (i.e., 1.2 wt%), as both the pore size and the surface area decreased (Table S1). A large-sized inter-nanoparticle spacing is expected to facilitate the penetration of perovskites inside the pores,[4] which is advantageous for absorbing incident photons and transporting charge carriers throughout the mesoporous electrode. The current density–voltage (*J–V*) characteristics of $CH_3NH_3PbI_3$ perovskite solar cells based on $NaYF_4$:Yb/Er mesoporous electrodes (i.e., 50 nm thick) with varied pore sizes are shown in Figure 3c. The corresponding photovoltaic parameters are summarized in Table S1. The open-circuit voltage, V_{oc}, short-circuit current density, J_{sc}, and fill factor, *FF*, of the devices were obviously enhanced with the increase of the pore sizes, and the PCEs were improved from 10.5% to 14.2% when the average pore size exceeded 30 nm.

The thickness effect of the $NaYF_4$:Yb/Er mesoporous film on the photovoltaic performance of $CH_3NH_3PbI_3$ perovskite solar cells was further scrutinized to optimize the device efficiency. Figure 3d compares the *J–V* characteristics of $CH_3NH_3PbI_3$ perovskite solar cells with different thicknesses of $NaYF_4$:Yb/Er mesoporous electrodes (i.e., with 0.8 wt% PEO additive). Compared to the planar device with an architecture of FTO/compact-TiO_2/$CH_3NH_3PbI_3$/Spiro-MeOTAD/Ag, the introduction of a $NaYF_4$:Yb/Er mesoporous layer between the compact TiO_2 and $CH_3NH_3PbI_3$ layers markedly increased the average PCE from 8.1% for the planar device to 14.2% for the mesoporous one. The optimized thickness of the $NaYF_4$:Yb/Er mesoporous layer was found to be about 150 nm, leading to a V_{oc} of 1.06 V, a J_{sc} of 22.1 mA cm^{-2}, a *FF* of 73.4%, and a high PCE of 17.2%. A further increase in the layer thickness from 150 nm to 350 nm led to the reduction in J_{sc}, V_{oc}, and PCEs, which were probably due to the increased R_s correlated with the insulating nature of $NaYF_4$:Yb/Er UCNPs (Table S2). The best $NaYF_4$:Yb/Er mesoporous solar cell showed a V_{oc} of 1.06 V, a J_{sc} of 22.6 mA cm^{-2}, a *FF* of 73.9%, and thus a PCE of 17.8%, which is comparable with that of the reference solar cell (i.e., PCE of 16.8%) fabricated by employing TiO_2 mesoporous electrodes (Figure S7a), and no serious hysteresis effects were observed in these devices (Figure S8). These high efficiencies signified that the $NaYF_4$:Yb/Er mesoporous layer can effectively serve as a scaffold to facilitate the growth of $CH_3NH_3PbI_3$ crystals during the two-step deposition process, similar to the function of TiO_2 and Al_2O_3 mesoporous electrodes in perovskite solar cells.[27]

To elucidate the interfacial charge-transfer properties of the $NaYF_4$:Yb/Er UCNP mesoporous electrodes, electrochemical impedance spectroscopy (EIS) measurements were performed. The Nyquist plot and corresponding equivalent circuit are shown in Figure S7b. The $NaYF_4$:Yb/Er mesoporous electrode was found to possess comparable series resistance R_s and contact resistance R_{co} with those of the TiO_2 mesoporous electrode (Table S3). However, a slightly higher R_{rec} for the $NaYF_4$:Yb/Er mesoporous electrode may be ascribed to the existence of fewer surface trap states in the insulating $NaYF_4$:Yb/Er than in the semiconducting TiO_2.[28] Compared to the TiO_2 mesoporous film-based device, the incident photo-to-electron conversion efficiency (IPCE) of a perovskite solar cell incorporating a $NaYF_4$:Yb/Er mesoporous electrode exceeded 85% over a broad range of 400–700 nm and suggested a better light harvesting and a lower charge recombination (Figure S7c). The characteristic of low charge recombination in the $NaYF_4$:Yb/Er mesoporous film-based device was consistent with the EIS result. We note that the J_{sc} of 21.2 mA cm^{-2} obtained from the integration of the IPCE profile was very close to the measured value of 22.6 mA cm^{-2}.

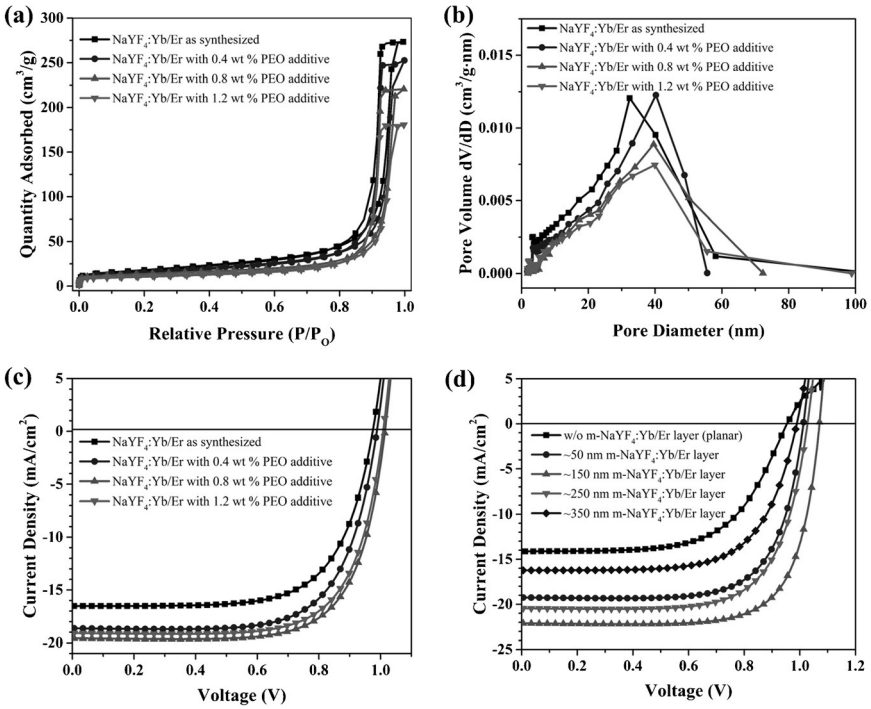

Figure 3. a) The nitrogen adsorption–desorption isotherms of $NaYF_4$:Yb/Er mesoporous films and b) the corresponding pore-size distributions. c) The current density–voltage (*J–V*) characteristics of $CH_3NH_3PbI_3$ solar cells using $NaYF_4$:Yb/Er mesoporous layers with varied ratios of PEO additives. d) The *J–V* characteristics of $CH_3NH_3PbI_3$ solar cells fabricated on different thicknesses of $NaYF_4$:Yb/Er mesoporous layers.

Theoretical studies have demonstrated that one promising avenue to promote the contribution of upconversion fluorescence to photocurrent is to operate solar cells under the concentrated solar power.[13,29,30] To date, the world record efficiency of 46% has been obtained in a multi-junction solar cell at a concentration of 508 suns, wherein the sub-cells effectively convert the incident photons in the range of 300–1750 nm into photocurrents.[31] As a proof of principle, the $NaYF_4$:Yb/Er mesoporous electrode-based perovskite solar cell was tested under a 980 nm NIR laser with a power of 2 W and a beam diameter of 0.3 cm (i.e., a power density of 28 W c^{-2}). The *J–V* characteristics in Figure 4a unambiguously showed that the $NaYF_4$:Yb/Er mesoporous electrode rendered $CH_3NH_3PbI_3$ perovskite solar cell to respond under concentrated NIR light, resulting in a V_{oc} of 0.89 V, a J_{sc} of 0.74 mA cm^{-2}, a *FF* of 53.9%, and a PCE of 0.35%. The *J–V* curve of the reference cell constructed with TiO_2 mesoporous electrode (i.e., the black curve) for comparison is also shown in Figure 4a, exhibiting no photovoltaic response under NIR illumination. This was consistent with the observations that bright green fluorescence can be seen on the $NaYF_4$:Yb/Er mesoporous electrode irradiated with the 980 nm NIR laser, while no fluorescence emerged on the TiO_2 mesoporous electrode due to the absence of the upconversion effect (Figure S9). When applying the 980 nm NIR laser on the $CH_3NH_3PbI_3$ perovskite solar cells with the $NaYF_4$:Yb/Er mesoporous electrode, which was simultaneously measured under an AM1.5G standard sunlight, the photocurrent density was increased from 22.7 mA cm^{-2} to 23.1 mA cm^{-2} due to the upconversion effect, thus promoting the device efficiency from 17.8% to 18.1% (Figure 4b). The photocurrent density and the corresponding PCE of the $NaYF_4$:Yb/Er mesoporous electrode-based perovskite solar cell were measured as a function of time at a constant forward bias of 0.875 V under an AM1.5G standard sunlight, during which the 980 nm NIR laser was switched on and off every 15 s as

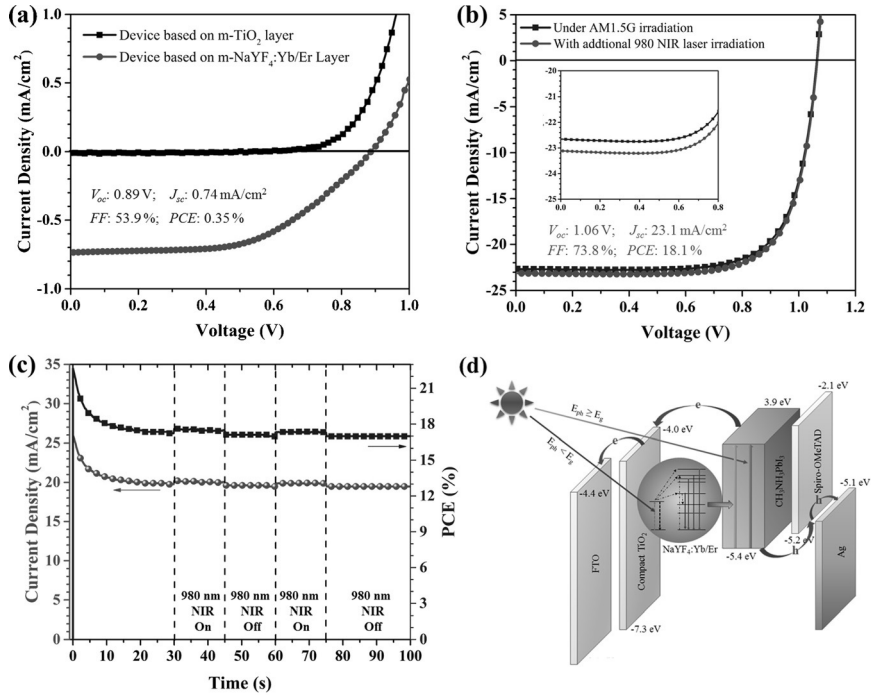

Figure 4. a) The current density–voltage (*J–V*) characteristics of $CH_3NH_3PbI_3$ solar cells using $NaYF_4$:Yb/Er UCNPs under 980 nm NIR laser light and b) the highest efficiencies under an AM1.5G standard sunlight and an additional 980 nm NIR laser. c) The photocurrent density and the corresponding efficiency of the $CH_3NH_3PbI_3$ solar cells capitalizing on $NaYF_4$:Yb/Er mesoporous electrodes with 980 nm NIR laser light switched on and off every 15 s. d) Scheme of the energy transfer process in $CH_3NH_3PbI_3$ solar cells using the $NaYF_4$:Yb/Er mesoporous electrodes.

shown in Figure 4c. A stable output photocurrent density of 19.5 mA cm^{-2} and the PCE of 17.0% can be maintained for 100 s under the standard sunlight, and the photocurrent density was increased to 19.9 mA cm^{-2} with a stable output PCE of 17.3% once the 980 nm NIR laser was turned on. The incorporation of upconversion nanoparticles provides a promising route to reducing the non-absorption photon loss in organolead halide perovskite solar cells, where incident photons with the energy higher than the band gap of perovskites (e.g., 1.6 eV for $CH_3NH_3PbI_3$) are effectively harvested by the perovskite active layer (Figure 4d), while incident photons with energy lower than the bandgap of perovskites (e.g., NIR light) are absorbed by the upconversion nanoparticles, followed by transferring to high-energy photons and in turn contributing to the photocurrents of perovskite active layers.

In summary, we demonstrated the implementation of monodisperse UCNPs for high-efficiency organolead halide perovskite solar cells. Uniform β-phase $NaYF_4$:Yb/Er UCNPs were created by employing a designed double hydrophilic star-like PAA-*b*-PEO diblock copolymer as nanoreactor. Quite intriguingly, the exploitation of $NaYF_4$:Yb/Er UCNPs as mesoporous electrode in $CH_3NH_3PbI_3$ perovskite solar cells imparted not only the growth of high-quality $CH_3NH_3PbI_3$ cuboid crystals by functioning as a scaffold yielding a high PCE of 17.8%, but also the realization of NIR perovskite solar cell under the 980 nm laser irradiation resulting in a PCE of 0.35% by harvesting the NIR solar photons (i.e., dual functionalities). Notably, the hydrophilic nature and long-chain characteristic of PEO ligands facilitated the fabrication of $NaYF_4$:Yb/Er UCNPs into mesoporous electrodes with tunable pore sizes for $CH_3NH_3PbI_3$ perovskite solar cells. This study provided a proof of principle of introducing upconversion materials as a dual-functional constituent of organolead halide perovskite solar cells for broadening the solar spectral use to NIR light, minimizing the non-absorption energy loss, and ultimately promoting the photovoltaic performance.

Acknowledgements

We gratefully acknowledge funding support from the Air Force Office of Scientific Research (grant number FA9550-13-1-0101) and National Science Foundation (grant number ECCS-1305087).

Keywords: near-infrared · photovoltaic devices · polymers · solar cells · upconversion nanoparticles

How to cite: *Angew. Chem. Int. Ed.* **2016**, *55*, 4280–4284
Angew. Chem. **2016**, *128*, 4352–4356

[1] A. Kojima, K. Teshima, Y. Shirai, T. Miyasaka, *J. Am. Chem. Soc.* **2009**, *131*, 6050.
[2] H. S. Kim, C. R. Lee, J. H. Im, K. B. Lee, T. Moehl, A. Marchioro, S. J. Moon, R. Humphry-Baker, J. H. Yum, J. E. Moser, M. Gratzel, N. G. Park, *Sci. Rep.* **2012**, *2*, 591591.
[3] M. Liu, M. B. Johnston, H. J. Snaith, *Nature* **2013**, *501*, 395.
[4] J. Burschka, N. Pellet, S. J. Moon, R. Humphry-Baker, P. Gao, M. K. Nazeeruddin, M. Gratzel, *Nature* **2013**, *499*, 316.
[5] W. S. Yang, J. H. Noh, N. J. Jeon, Y. C. Kim, S. Ryu, J. Seo, S. I. Seok, *Science* **2015**, *348*, 1234.
[6] M. Xiao, F. Huang, W. Huang, Y. Dkhissi, Y. Zhu, J. Etheridge, A. Gray-Weale, U. Bach, Y. B. Cheng, L. Spiccia, *Angew. Chem. Int. Ed.* **2014**, *53*, 9898; *Angew. Chem.* **2014**, *126*, 10056.
[7] H. P. Zhou, Q. Chen, G. Li, S. Luo, T. B. Song, H. S. Duan, Z. R. Hong, J. B. You, Y. S. Liu, Y. Yang, *Science* **2014**, *345*, 542.
[8] K. Wang, C. Liu, C. Yi, L. Chen, J. H. Zhu, R. A. Weiss, X. Gong, *Adv. Funct. Mater.* **2015**, *25*, 6875.
[9] N. J. Jeon, J. H. Noh, W. S. Yang, Y. C. Kim, S. Ryu, J. Seo, S. I. Seok, *Nature* **2015**, *517*, 476.
[10] Y. J. Fang, Q. F. Dong, Y. C. Shao, Y. B. Yuan, J. S. Huang, *Nat. Photonics* **2015**, *9*, 679.
[11] X. Y. Huang, S. Y. Han, W. Huang, X. G. Liu, *Chem. Soc. Rev.* **2013**, *42*, 173.
[12] W. Q. Zou, C. Visser, J. A. Maduro, M. S. Pshenichnikov, J. C. Hummelen, *Nat. Photonics* **2012**, *6*, 560.
[13] V. Badescu, A. M. Badescu, *Renewable Energy* **2009**, *34*, 1538.
[14] A. Shalav, B. S. Richards, T. Trupke, K. W. Kramer, H. U. Gudel, *Appl. Phys. Lett.* **2005**, *86*, 013505.
[15] G. B. Shan, G. P. Demopoulos, *Adv. Mater.* **2010**, *22*, 4373.
[16] J. S. Liu, T. Tanaka, K. Sivula, A. P. Alivisatos, J. M. J. Frechet, *J. Am. Chem. Soc.* **2004**, *126*, 6550.
[17] L. Zhao, X. C. Pang, R. Adhikary, J. W. Petrich, Z. Q. Lin, *Adv. Mater.* **2011**, *23*, 2844.
[18] J. Xu, J. Wang, M. Mitchell, P. Mukherjee, M. Jeffries-EL, J. W. Petrich, Z. Q. Lin, *J. Am. Chem. Soc.* **2007**, *129*, 12828.
[19] L. Zhao, Z. Q. Lin, *Adv. Mater.* **2012**, *24*, 4353.
[20] L. Zhao, X. C. Pang, R. Adhikary, J. W. Petrich, Z. Q. Lin, *Angew. Chem. Int. Ed.* **2011**, *50*, 3958; *Angew. Chem.* **2011**, *123*, 4044.
[21] A. Stavrinadis, R. Beal, J. M. Smith, H. E. Assender, A. A. R. Watt, *Adv. Mater.* **2008**, *20*, 3105.
[22] X. C. Pang, L. Zhao, W. Han, X. K. Xin, Z. Q. Lin, *Nat. Nanotechnol.* **2013**, *8*, 426.
[23] H. Xu, Y. Xu, X. Pang, Y. He, J. Jung, H. Xia, Z. Lin, *Sci. Adv.* **2015**, *1*, e1500025.
[24] V. Caramia, I. S. Bayer, G. C. Anyfantis, R. Ruffilli, F. Ayadi, L. Martiradonna, R. Cingolani, A. Athanassiou, *Nanotechnology* **2013**, *24*, 055602.
[25] G. S. Yi, G. M. Chow, *Adv. Funct. Mater.* **2006**, *16*, 2324.
[26] J. H. Im, I. H. Jang, N. Pellet, M. Gratzel, N. G. Park, *Nat. Nanotechnol.* **2014**, *9*, 927.
[27] S. Kazim, M. K. Nazeeruddin, M. Gratzel, S. Ahmad, *Angew. Chem. Int. Ed.* **2014**, *53*, 2812; *Angew. Chem.* **2014**, *126*, 2854.
[28] M. M. Lee, J. Teuscher, T. Miyasaka, T. N. Murakami, H. J. Snaith, *Science* **2012**, *338*, 643.
[29] T. Trupke, M. A. Green, P. Wurfel, *J. Appl. Phys.* **2002**, *92*, 4117.
[30] V. Badescu, *J. Appl. Phys.* **2008**, *104*, 113120.
[31] M. A. Green, K. Emery, Y. Hishikawa, W. Warta, E. D. Dunlop, *Prog. Photovoltaics* **2015**, *23*, 1.

Received: January 27, 2016
Published online: February 19, 2016

